

## Acoustic coupling at multiple interfaces and the liquid phase response of the thickness shear-mode acoustic wave sensor

Jonathan S. Ellis<sup>a</sup> and Michael Thompson<sup>\*b</sup>

<sup>a</sup> Institute of Biomaterials and Biomedical Engineering, University of Toronto, 4 Taddle Creek Road, Toronto, Ontario M5S 3G9, Canada

<sup>b</sup> Department of Chemistry, University of Toronto, 80 St. George Street, Toronto, Ontario M5S 3H6, Canada. E-mail: mikethom@chem.utoronto.ca

Received (in Cambridge, UK) 24th February 2004, Accepted 22nd April 2004

First published as an Advance Article on the web 7th May 2004

**Interfacial slip at two interfaces is included in an acoustic wave model for a transverse-shear mode (TSM) device, coated with a thin viscoelastic film in contact with a liquid, producing series resonant frequency ( $f_s$ ) and motional resistance ( $R_m$ ) shifts in the same direction.**

High-frequency acoustic wave devices provide a highly sensitive and informational technique for the on-line detection of biochemical binding events involving proteins, nucleic acids and cells.<sup>1</sup> The most common such structure is the AT-cut transverse-shear mode (TSM) sensor, which is comprised of a thin quartz wafer with electrodes on both sides. The electric field generated by the electrodes piezoelectrically induces acoustic shear waves in the thickness direction. A biomolecular film is attached to one face of the sensor, which is then incorporated into a flow-injection configuration. Alternatively, such layers can be introduced in an on-line fashion. The shear wave propagates through the film and into the liquid, and can be characterised from the storage and dissipation properties of the device. The electrical impedance of the sensor is measured and related to the complex acoustic impedance. The imaginary part represents energy storage and is proportional to a change in resonant frequency  $f_s$ , while energy dissipation, the real component, is related to the  $Q$ -factor or motional resistance,  $R_m$ , of the device. Generally,  $f_s$  and  $R_m$  vary in opposite directions.

The series resonant frequency  $f_s$  depends on the location of the effective reflecting interface, or the wavelength  $\lambda_{\text{eff}}$ , of the resonant standing wave. In a typical configuration, the sensor is comprised of quartz and electrodes, a linker, a receptor and a contacting fluid. The linker and receptor layers are normally lumped together into a composite film. A standing shear wave is propagated and reflected in the thickness direction through the quartz, metal and film layers, with some of the acoustic energy lost viscously to the fluid layer. At steady-state resonance, the amount of energy emitted by the quartz will equal the energy reflected at the film–liquid interface, plus the energy lost to the liquid.<sup>2</sup> The location of the reflecting surface determines  $f_s$ .

Viscous interactions lead to reflections over the entire thickness of the film and adjacent fluid, causing a flattening and broadening of the impedance spectrum of the resonant wave. This lowers the  $Q$ -factor of the device, which is inversely proportional to  $R_m$ . The typical increase in  $R_m$  accompanying the decrease in  $f_s$  is due to the increase in viscoelastic interactions within the film as the acoustic wave propagates through it. Provided that the acoustic wave does not vanish in the film, more dissipative interactions occur as the thickness increases, further broadening the impedance spectrum.

Recently, we have observed experimental shifts in  $f_s$  and  $R_m$  that occur in the same direction.<sup>3</sup> These studies involve proteins and oligonucleotides attached to the surface of the device electrode through a linking moiety. In the case of such multi-layered structures, interfacial coupling plays an important role. If the interaction between any two layers changes over the course of a binding event, the amount of acoustic energy propagated into the upper layer will also vary, resulting in a change in the acoustic signal. Changes in coupling can lead to interfacial slip, whereby the no-slip boundary condition of classical hydrodynamics is relaxed. In this scenario, the relative velocity of particles on either side of an interface is allowed to vary. In the case where multiple interfaces

are present, slip has been proposed as a possible mechanism to explain experimental shifts of  $f_s$  and  $R_m$  in the same direction.<sup>4</sup>

When describing slip at multiple interfaces, the choice of model is important because film–liquid (outer) slip may be physically different than substrate–film (inner) slip. Ferrante *et al.*<sup>5</sup> used a complex displacement slip boundary condition to describe slip at the liquid–surface interface, where the complex value allows differences in magnitude and phase between the layers. Hayward and Thompson<sup>6</sup> extended this model to slip at multiple interfaces. Two recent analyses<sup>7,8</sup> have shown that the real-valued slip length  $b$  describes solid–liquid slip on a TSM device. Rodahl and Kasemo<sup>9</sup> applied slip through the shear stress boundary condition using a single friction value, which was extended to multiple layers by McHale *et al.*<sup>4</sup> In a recent analysis, Lu *et al.*<sup>10</sup> have shown that in certain limits, displacement and shear boundary conditions describe the same situation.

Inner slip, between a solid substrate and an attached film, requires a different description. The film–substrate bonds are generally more viscoelastic than a surface–liquid interface, where only viscous losses occur. Energy can be transmitted elastically through strongly-adhered bond, as well as viscously. True slip, in the sense of a planar discontinuity between layers, may not occur at inner layers, but viscoelastic slip can be used to describe the substrate–film interface.

In the present paper, we use the four-layer model of Hayward and Thompson<sup>6</sup> with slip applied at the film–liquid (outer slip) and substrate–film (inner slip) interfaces. We then further examine the behaviour of the complex-valued inner slip model. Outer slip is modelled using the slip length  $b$  and varied between 0 (no-slip) and 30 nm (strong slip). For a viscoelastic layer attached to the substrate, the complex slip can also be modelled with a single, real value using a viscous friction law.<sup>11</sup> The slip parameter between the substrate and the film is

$$\alpha_{\text{inner}} = v_{\text{film}}/v_{\text{subs}} = (1 + i\omega\tau)^{-1}, \quad (1)$$

where  $\omega$  is the frequency and  $\tau$  is the slip relaxation time, which is the ratio of viscous to elastic contributions to the interfacial behaviour. This approach provides a physical description of the relative motion at the interface, such that both magnitude,  $|\alpha|$ , and phase,  $\angle\alpha$ , can be modelled. The interface has its own relaxation time, independent of the internal film viscoelasticity, which describes the response of the film with respect to the motion of surface. Varying  $\omega\tau$  from 0 to 50, as in McHale *et al.*<sup>4</sup> corresponds to changing the viscoelastic nature of the film from a viscous liquid to an amorphous (glassy) solid. However, biopolymers in liquid are probably more fluid-like, so a value between 0 and 1 is more likely. This is equivalent to the inner slip parameter  $\alpha_{\text{inner}}$  varied between  $1\angle 0^\circ$  and  $0.707\angle -45^\circ$ .

Fig. 1 shows theoretical calculations of  $f_s$  and  $R_m$  for a 9-MHz TSM device with a 5 nm film (density  $\rho_f = 1.2 \text{ g}\cdot\text{cm}^{-3}$ , viscosity  $\eta_f = 366 \text{ cP}$ , stiffness  $\mu_f = 1 \text{ MPa}$ ), and slip at both the inner and outer interfaces. Changes in the same direction can be generated in two different ways using this model. The first is associated with the maximum in the  $R_m$  plot, whereby if outer slip is held constant, and  $\omega\tau$  is between 0 and 0.5, any change in slip will result in an increase in both  $f_s$  and  $R_m$ . The second occurs if inner slip increases as outer slip decreases. For any value of slip, both  $f_s$  and  $R_m$  will increase.

It is important to note that this treatment is equivalent to McHale *et al.*<sup>4</sup> where the authors found that shifts of  $f_s$  and  $R_m$  in the same direction were possible with two viscoelastic layers with slip. We have used a substrate coated with three films, two viscoelastic and one purely viscous, with slip at the upper film–liquid interface. The lower film is vanishingly thin to model interfacial bonds, with viscoelastic properties represented by the slip relaxation time  $\omega\tau$ .

Modelling inner slip with eqn. (1) provides a mathematical explanation of  $f_s$  and  $R_m$  shifts in the same direction. However, this does not elucidate the physical mechanisms. With eqn. (1), the inner slip is determined by a single factor  $\omega\tau$ , corresponding to a viscous friction law. When this is applied to the equations of motion, it actually generates two factors, the magnitude and phase of the relative motion of the film and substrate, which in this case are varied between 0.707 and 1, and  $0^\circ$  and  $-45^\circ$ , respectively. To examine the relative influence of each on the  $f_s$  and  $R_m$  responses, the magnitude and phase are varied independently. Fig. 2 shows the behaviour of  $f_s$  and  $R_m$  as  $|\alpha_{\text{inner}}|$  is varied between 0.7 and 1, at constant phase,  $\angle\alpha_{\text{inner}} = 0^\circ$ . The model behaves classically, where  $f_s$  and  $R_m$  vary in opposite directions as the strength of the slip is increased. Fig. 3 shows the acoustic behaviour as  $\angle\alpha_{\text{inner}}$  is varied between  $0^\circ$  and  $-45^\circ$ , at constant  $|\alpha_{\text{inner}}| = 1$ . The origin of the shifts in the same direction of  $f_s$  and  $R_m$  becomes apparent. Both  $f_s$  and  $R_m$  decrease as the inner slip phase angle increases.

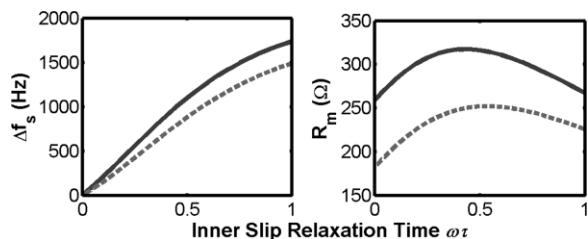


**Fig. 1** Values of  $f_s$  and  $R_m$  as inner and outer slip are varied. The horizontal axis shows the variation in inner slip, while changes in outer slip are represented by the dashed lines. The solid lines indicates  $b = 0$  nm and the dashed line is  $b = 30$  nm. Inner slip increases as  $\omega\tau$  increases, and outer slip increases with increasing slip length  $b$ .

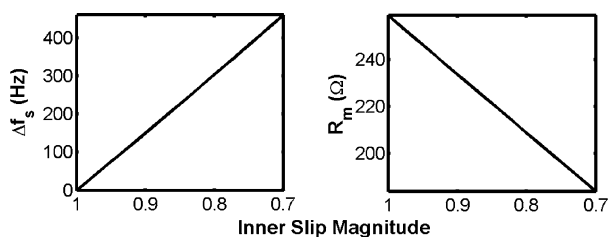


**Fig. 2** Change in  $f_s$  and  $R_m$  values as the inner slip magnitude  $|\alpha|$  is varied from no-slip ( $|\alpha| = 1$ ) to strong slip ( $|\alpha| = 0.7$ ) for phase angle  $\angle\alpha = 0^\circ$ .

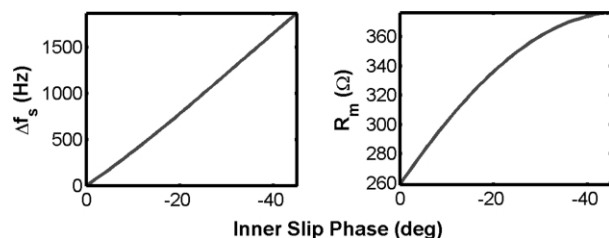


**Fig. 3** Change in  $f_s$  and  $R_m$  values as the inner slip phase  $\angle\alpha$  is varied from no-slip ( $\angle\alpha = 0^\circ$ ) to strong lag ( $\angle\alpha = -45^\circ$ ) for magnitude  $|\alpha| = 1$ .

This behaviour provides insight into the mechanism governing the shifts in  $f_s$  and  $R_m$ . As the phase lag between the two surfaces increases, both  $f_s$  and  $R_m$  increase. From Ferrante *et al.*<sup>5</sup> the chemical bond at the interface can be viewed as a mass on top of a flexible spring, where the base of the spring is oscillating in the horizontal direction. The spring is massless, since it represents the chemical bond across the interface. The increased lag is due to a reduction in the “stiffness” of the interfacial interaction, since a more compliant spring will deform more as it is stressed by the oscillating surface. As the rigidity of the bond decreases, less wave energy is propagated into the film since the compliant material cannot transfer wave energy to as great a distance as a stiffer material. In the case of an attached layer involving phase slip, the effective wavelength of the device,  $\lambda_{\text{eff}}$ , will be smaller than for the no-slip case and  $f_s$  will be higher. As the interfacial bonds become more compliant and cannot support as much acoustic energy, the substrate must do more work to sustain the oscillation of the upper mass. In effect, it is expending more energy to move the mass the same distance through the surrounding space than would be required for a rigid bond, which appears as energy dissipation in moving the mass through the surrounding fluid. This results in the observed increases of both  $f_s$  and  $R_m$ .

In summary, we have shown theoretically that by including slip at the interfaces of a typical configuration of a TSM acoustic wave device operating in liquid, we can generate non-classical shifts in  $f_s$  and  $R_m$ . In fact, these results can be produced by simply varying the inner slip phase angle, so the extra degree of freedom added by including slip at both interfaces may not be necessary in some cases. However, in biochemical applications, changes in slip may occur at both interfaces, making two real slip parameters physically necessary. We can also consider slip as a stochastic de-coupling between strongly adhered particles, whereby changes in the lability of substrate–film interfacial bonds<sup>12</sup> may result in apparent slip behaviour. These ideas demonstrate that the classical notion of this device as a pure microbalance (*viz.* the oft-quoted “QCM”) is flawed, but also confirms the potential of acoustic wave physics as a sensitive and powerful tool for biophysicists and bioanalytical chemists.

We are indebted to the Natural Sciences and Engineering Research Council of Canada and an Ontario Graduate Scholarship for support of this work. Also, we gratefully acknowledge G. Hayward of the University of Guelph for many helpful and stimulating discussions and M. Zhang of the University of Toronto for his help with graphical work.

## References

- B. A. Cavic, G. L. Hayward and M. Thompson, *Analyst*, 1999, **124**, 1405.
- A. L. Kipling and M. Thompson, US Patent 5,374,521, Dec. 20, 1994.
- N. Tassew and M. Thompson, *Anal. Chem.*, 2002, **74**, 5313; E. L. Lyle, G. L. Hayward and M. Thompson, *Analyst*, 2002, **127**, 1596; C. N. Jayarajah and M. Thompson, *Abstr. Pap. Am. Chem. Soc.*, 2002, **224**, U445.
- G. McHale, R. Lucklum, M. I. Newton and J. A. Cowen, *J. Appl. Phys.*, 2000, **88**, 7304.
- F. Ferrante, A. L. Kipling and M. Thompson, *J. Appl. Phys.*, 1994, **76**, 3448.
- G. L. Hayward and M. Thompson, *J. Appl. Phys.*, 1998, **83**, 2194.
- J. S. Ellis and G. L. Hayward, *J. Appl. Phys.*, 2003, **94**, 7856.
- J. S. Ellis, G. McHale, G. L. Hayward and M. Thompson, *J. Appl. Phys.*, 2003, **94**, 6201.
- M. Rodahl and B. Kasemo, *Sens. Actuators, A-Phys.*, 1996, **54**, 448.
- F. Lu, H. P. Lee and S. P. Lim, *Smart Mater. Struct.*, 2003, **12**, 881.
- E. D. Smith, M. O. Robbins and M. Cieplak, *Phys. Rev. B*, 1996, **54**, 8252.
- D. A. Hutt, E. Cooper and G. J. Leggett, *J. Phys. Chem. B*, 1998, **102**, 174; N. J. Brewer, R. E. Rawsterne, S. Kothari and G. J. Leggett, *J. Am. Chem. Soc.*, 2001, **123**, 4089.